Multichannel Time-Frequency Complexity Measures for the Analysis of Age-Related Changes in Neuromagnetic Resting-State Activity

Marcelo A. Colominas, Vincent Wens, Alison Mary, Nicolas Coquelet, Mohamad El Sayed Hussein Jomaa, Nisrine Jrad, Anne Humeau-Heurtier and Patrick Van Bogaert

***Abstract*—We propose new multichannel time-frequency complexity measures to evaluate differences on magnetoencephalograpy (MEG) recordings between healthy young and old subjects at rest at different spatial scales. After reviewing the Rényi and singular value decomposition entropies based on time-frequency representations, we introduce multichannel generalizations, using multilinear singular value decomposition for one of them. We test these quantities on synthetic data, illustrating how the introduced complexity measures focus on number of components, nonstationarity and similarity across channels. Friedman tests are used to confirm the differences between young and old groups, and heterogeneity within groups. Experimental results show a consistent increase in complexity measures for the old group. When analyzing the topographical distribution of complexity values, we found clusters in the frontal sensors. The complexity measures here introduced seem to be a better indicator of the neurophysiologic changes of aging than power envelope connectivity. Here we applied new multichannel time-frequency complexity measures to resting-state MEG recordings from healthy young and old subjects. We showed that these features are able to reveal regional clusters. The multichannel time-frequency complexities can be used to monitor the aging of subjects. They also allow a mutual information approach, and could be applied to a wider range of problems.**

***Index Terms*—MEG data, aging, Rényi entropy, signal complexity, SVD entropy, time-frequency, multichannel.**

I. Introduction

VARIOUS approaches may be used to study the evolution of brain function over the lifespan in healthy subjects. One approach consists in searching coordinated activity between different brain areas. This is the basic principle of functional connectivity [1], that may be studied either indirectly using functional magnetic resonance imaging (fMRI) to measure local variations of brain perfusion that are thought to reflect neuronal activity, or through direct measures of neurophysiological signals recorded by electroencephalography (EEG) or magnetoencephalography (MEG) [2], [3], [4]. MEG is a technique that records the magnetic fields produced by electrical currents in the brain and enables investigating noninvasively neuronal activity with a time resolution at the order of the millisecond and a spatial discrimination of 2-3 mm, at least under favorable circumstances [5], [6].

Several studies performed using fMRI have shown changes of resting-state functional connectivity with age in various large-scale networks. These changes most often consist in decreased connectivity between nodes of brain networks, but increased connectivity also occur (for a review, see [7]). Age-related changes might also be looked for in MEG recordings. Fernández *et al.* found significant increases in Lempel-Ziv complexity measures with age [8]. Shumbayawonda *et al.* confirmed increases in permutation entropy with age [9], and in permutation Lempel-Ziv complexity with age [10]. By contrast, Coquelet *et al.* did not find any significant age-related changes in both static and dynamic power envelope-based connectivity from resting-state MEG data, suggesting that the electrophysiological connectome is maintained in healthy aging [4]. As MEG power envelope connectivity is the best known electrophysiological correlate of fMRI resting-state networks [11], [12], [13], this absence of age-related changes might be related to neurovascular coupling alteration [4].

The assessment of functional connectivity from power envelope provides only one aspect of the rich dynamics of MEG signals. Another approach to search for lifespan variations from EEG/MEG signals is to assess time-frequency (TF) complexity [14], [15], which measures the information content of a time-frequency representation of the signal, exploring the time-varying spectral content without band-passing the signal into the classical frequency bands. Because of that, the results are not confined to a specific band (which might lead to different results for different bands) but reflects the richness of all the frequency content.

In a previous work [15], the ability of the time-frequency Rényi and Singular Value Decomposition (SVD) entropies to evidence differences in complexities on EEG recordings from epileptic patients before and after medication were reported. Here we introduce multichannel versions of these two complexity measures, and apply them on MEG recordings

M. A. Colominas, M. El Sayed Hussein Jomaa, N. Jrad, A. Humeau-Heurtier and P. Van Bogaert are with Univ. Angers, LARIS - Laboratoire Angevin de Recherche en Ingénierie des Systèmes, 62 avenue Notre-Dame du Lac, 49000 Angers, France (correspondence e-mail: marcelo.colominas@univ-angers.fr).

V. Wens and N. Coquelet are with LCFC - Laboratoire de Cartographie Fonctionnelle du Cerveau, UNI - ULB Neurosciences Institute, Université Libre de Bruxelles (ULB), Brussels, Belgium.

V. Wens is also with Magnetoencephalography Unit, Department of Functional Neuroimaging, Service of Nuclear Medicine, CUB - Hôpital Erasme, Brussels, Belgium.

A. Mary is with Normandie Univ., UNICAEN, PSL Research University, EPHE, INSERM, U1077, CHU de Caen, Neuropsychologie et Imagerie de la Mémoire Humaine, Caen, France.

N. Jrad is also with Université Catholique de l'Ouest, Angers-Nantes, France.

P. Van Bogaert is also with the Department of Pediatric Neurology, CHU Angers, France.

from healthy young and old subjects, using the same MEG data sets from [4], which will allow us to discuss our results in comparison with theirs. We hypothesize that differences might be found not only at "fine scales" (i.e. analyzing every sensor individually) but also at "coarse scales" (aggregation of sensors). This is especially relevant in our case since we deal with healthy adult subjects who do not presented any sign of cognitive decline, and for whom no changes in resting-state networks were found [4]. However, there exists cooperative phenomena at larger scales [16], [17], [18] that we want to explore *via* our new multichannel approaches. We also want to explore the distribution of complexity *within* each group. How spatial homogeneity of complexity compares in both groups? Are the entropy values evenly distributed or they form some clusters? To dig into it, we perform statistical tests within each group to look for sensors with outstanding entropy values.

The paper is organized as follows. In Sec. II we recall definitions of the existing time-frequency complexity measures and introduce multichannel versions, illustrating their capabilities on artificial signals. In Sec. III we describe our experiments on real MEG data and present the main results. We offer a discussion in Sec. IV, and Sec. V concludes the paper.

II. Multichannel Time-Frequency Entropies

The *multicomponent signals* consist of a superposition of a small number of components modulated both in amplitude and frequency (AM-FM), and are a versatile way to model phenomena such as audio signals [19], biomedical signals [20], or economic temporal series [21].

A signal made of L components can be written as:

$$x(t) = \sum_{l=1}^{L} a_l(t)\ \cos(2\pi\phi_l(t)), \tag{1}$$

with $a_l(t), \phi_l'(t) > 0\,\forall t$, where $\phi'(t)$ is the time derivative of $\phi(t)$. For the multicomponent model, the temporal variations of $a_l(t)$ and $\phi_l'(t)$ are small, which means: $|a_l'(t)|, |\phi_l''(t)| < \epsilon$, for a small $\epsilon > 0$. The signals modeled as in (1) have a particular structure in the time-frequency plane: every component occupies a "ribbon" around its *instantaneous frequency* $\phi'(t)$ [22]. The more components we have, the more ribbons and the larger occupancy of the plane we will get. Let us analyze the signal (1) with the (modified) Short Time Fourier Transform (STFT)

$$F_x^g(t,f) = \int x(u)g(u-t)e^{-i2\pi f(u-t)}du, \tag{2}$$

where $g(t)$ is an even real compact-supported window with $\mathrm{supp}\{G(f)\} \subseteq [-B, +B]$ [1,2]. If the instantaneous frequencies $\phi_l'(t)$ are well separated (i.e. by at least $2B$ for all t) and $|a_l'(t)|, |\phi_l''(t)|$ are small, then each component "lives" in non overlapping ribbons, which leads to the spectrogram

$$S_x^g(t,f) = |F_x^g(t,f)|^2 \approx \sum_{l=1}^{L} a_l^2(t)|G(f-\phi_l'(t))|^2, \tag{3}$$

[1]This is only an approximation since the compact-supportness of g prevents G to have a compact support.

[2]$G(f) = \int g(t)e^{-i2\pi ft}dt$ is the Fourier transform of $g(t)$.

in which cross-component terms are negligible [23], [24]. Due to its symmetry for real signals, and for the sake of simplicity, we consider only positive frequencies for the spectrogram, and we will do so for the rest of this work.

A. Discrete-time implementations

When working on digital computers, what we have is a sampled version of the signal: $x[n] = x(n\Delta t)$, with $n \in \mathbb{N}$ and $\Delta t = 1/f_s$ the sampling period corresponding to the sampling frequency f_s. In this case, the STFT becomes

$$F_x^g[n,k] = \sum_u x[u]g[u-n]e^{-i2\pi k\Delta f(u-n)}, \tag{4}$$

with $k \in \mathbb{N}$ and Δf being the frequency resolution of the analysis. For finite time series, the time index n ranges from 1 to N. The frequency index k ranges from 1 to K (considering only positive frequencies as we already explained), with $K\Delta f = 1/2$ (the maximum possible normalized frequency).

B. Time-frequency entropies

The *time-frequency entropies* are complexity measures that are not applied directly on the signals but on a time-frequency representation (TFR), aiming at quantifying the amount of information in the time-frequency plane. A widespread manner to measure this information and complexity comes from the analogy between signal energy densities and probability densities [25], [14]. In this analogy, the instantaneous energy $|x(t)|^2$ and the spectral energy $|X(f)|^2$ act as unidimensional densities of the energy of the signal in time and frequency respectively, while the TFR of the signal would behave as a bidimensional energy density in time-frequency. Regardless of the considerations to be taken with respect to this analogy (see [14]), the Rényi entropy of the spectrogram (or other TFRs) $S_x^g[n,k] = |F_x^g[n,k]|^2$ is defined as

$$H_R^\alpha(S_x^g) = \frac{1}{1-\alpha}\log_2 \sum_n \sum_k \frac{(S_x^g[n,k])^\alpha}{(\sum_a \sum_b S_x^g[a,b])^\alpha}, \tag{5}$$

with $\alpha \neq 1$, where a, b are just auxiliary variables.

The Rényi entropy behaves in a similar way to the Shannon entropy (the latter being the particular case $\alpha \to 1$ of the former). For concentrated TFRs of signals made of a relatively small number of components (small L in (1) and (3)) the entropy would attain low values, while for scattered TFRs of more complicated signals it would take larger values. The "counting" property of the Rényi entropy for TFRs is properly detailed in [14], and it is one of the main reasons for which it is used as a measure of complexity and/or the amount of information in the TF plane. Moreover, a study of the Rényi entropy of the spectrogram of a multicomponent signal can be found in [26]. However, it should be remarked that this entropy seems to be rather transparent to the non-stationarity of the signal [15].

A different way to measure the complexity of the time-frequency plane is offered by the SVD entropy, introduced in [27] and used in the context of TFRs in [28]. The SVD of a TFR (the spectrogram in our case) expands it as

$$S_x^g[n,k] = \sum_j \sigma_j u_j[n]v_j[k], \tag{6}$$

This article has been accepted for publication in a future issue of this journal, but has not been fully edited. Content may change prior to final publication. Citation information: DOI 10.1109/JBHI.2019.2892823, IEEE Journal of Biomedical and Health Informatics

where $u_j[n]$ and $v_j[k]$ are vectors whose dyadic products form "basic" one-rank matrices which retrieve the original matrix when weighted summed. Then, a Shannon entropy formula is applied on the singular values σ_j's, after normalization:

$$H_V(S_x^g) = -\sum_j \frac{\sigma_j}{\sum_i \sigma_i} \log_2 \left(\frac{\sigma_j}{\sum_i \sigma_i} \right). \tag{7}$$

This complexity measure is more focused on the (non)stationarity of the signal. In a discrete case, the TFR becomes a matrix and the more linearly dependent are the columns, the lower is the SVD entropy value. So, for instantaneous frequencies $\phi'(t)$ that have little variations (the columns of the TFR are similar to each other) we expect lower values, and *vice versa*.

C. A multichannel setting

In the multichannel case, instead of a single signal we have a set of M signals:

$$\mathbf{x}[n] = \{x_m[n]\} = \{x_1[n], x_2[n], \ldots, x_M[n]\}, \tag{8}$$

and they should be processed jointly. This means that we must redefine Eqs. (5) and (7) in a multivariate way.

For every channel, we compute the STFT and the spectrograms to form a "stack" of TFRs:

$$S_{\mathbf{x}}^g[m,n,k] = \left| \sum_u x_m[u] g[u-n] e^{-i2\pi k \Delta f (u-n)} \right|^2. \tag{9}$$

For the Rényi entropy, a straightforward extension can be defined as

$$H_R^\alpha(S_{\mathbf{x}}^g) = \frac{1}{1-\alpha} \log_2 \sum_m \sum_n \sum_k \frac{(S_{\mathbf{x}}^g[m,n,k])^\alpha}{(\sum_a \sum_b \sum_c S_{\mathbf{x}}^g[a,b,c])^\alpha}, \tag{10}$$

where, as in Eq. (5), a, b, c are auxiliary variables. This entropy has a theoretical minimum possible value of 0, when all the energy is concentrated in a single time-frequency bin of a single channel; and a maximum value of $\log_2 MNK$, where M, N and K are, respectively, the total number of channels, time samples and frequency bins, when all the time-frequency bins for all the channels have the same value.

Extending the SVD entropy requires first to decompose the tensor $S_{\mathbf{x}}^g[m,n,k]$ of size $M \times N \times K$ using the multilinear SVD (MLSVD):

$$S_{\mathbf{x}}^g[m,n,k] = T \bullet_1 U^{(1)} \bullet_2 U^{(2)} \bullet_3 U^{(3)}, \tag{11}$$

where T is the core tensor, $U^{(d)}$ are the factor matrices and $\bullet_d$ stands for the tensor-matrix product in mode d [29], [30].

Unlike standard SVD, the tensor T is not diagonal. The multilinear singular values are defined as the Frobenius norms of the slices of order $D-1$ ($D=3$ being the dimension in our case) for the different modes, i.e. the norm of the subtensor created by fixing one index. This creates $D=3$ sets of singular values. We define the MLSVD entropy as:

$$H_V(S_{\mathbf{x}}^g) = -\sum_p \sum_j \frac{\sigma_j^{(p)}}{\sum_i \sigma_i^{(p)}} \log_2 \left(\frac{\sigma_j^{(p)}}{\sum_i \sigma_i^{(p)}} \right) \tag{12}$$

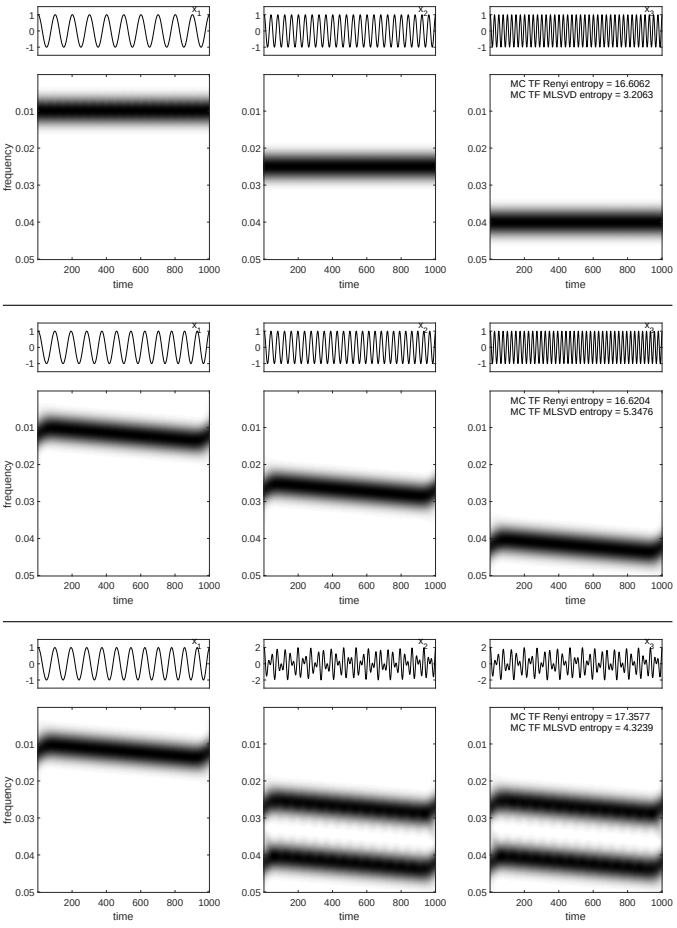

Fig. 1. Three multichannel signals with different levels of complexity. 1000 sample points. Spectrograms were performed with Hann window of 250 samples. $\alpha = 2$ for Rényi entropy. Top: one pure tone in each channel gives a relatively low value for our two measures. Middle: one linear chirp in each channel increases the MLSVD entropy almost without affecting the Rényi entropy. Bottom: the second and third channels have the same two-chirp composite signal increasing the Rényi entropy (more components overall) and retrieving an intermediate value for the MLSVD entropy.

where $\sigma^{(p)}$, with $p = 1, 2, 3$, stands for the sets of singular values. Similarly to the Rényi entropy, the maximum possible value is $\log_2 M + \log_2 N + \log_2 K = \log_2 MNK$.

D. Characteristics of the multichannel TF entropies

The properties of the time-frequency Rényi and SVD entropies were described in [15]. Generally speaking, the Rényi entropy behaves as a "counter" of components [14], regardless of their bandwidths. On the other hand, the SVD entropy focuses on the (non)stationarity of the signal.

The multichannel extension of the Rényi entropy (Eq. (10)) would consider all the components throughout the channels, counting them all. The MLSVD entropy (Eq. (12)) offers a more complex behavior: besides focusing on the nonstationarity of the components (i.e., variations on their instantaneous frequencies), it also considers *similarity* across the channels (in terms of time-frequency content). The more different the spectrograms are across channels, the higher value would the MLSVD entropy attain.

A series of examples of three-channel signals can be found in Fig. 1. One thousand points were used to generate the signals, and a Hann window of 250 samples was used for the spectrograms. The Rényi entropy was computed with $\alpha = 2$. At the very top, a simple three-channel signal with a pure tone for each of them, serves as a reference. The three pure tones have different frequencies. The values for the Rényi and MLSVD entropies are 16.61 and 3.21 respectively. In the middle row, the pure tones were replaced by linear chirps, all of them with the same chirp rate. The Rényi entropy remains almost unchanged (16.62) since there are still three components as in the previous case. The MLSVD entropy, however, notes the nonstationarity due to the frequency modulation, showing a substantially higher value (5.35). In the bottom row, the channels 2 and 3 have the same signal: a superposition of two linear chirps. The Rényi entropy increases (17.36) since we have five components overall instead of the three components of the previous cases. The MLSVD entropy takes an intermediate value (4.32) because of the similarity between channels 2 and 3. The nonstationarity of the components is balanced with the similarity between two channels.

III. Resting-State MEG Data

A. Database

The dataset used here is the same as in Coquelet *et al.*, in which the population characteristics and the acquisition procedures are detailed [4]. Briefly, twenty-five young (12 females and 13 males; age: 23.6 $\pm$ 2.9 years; age range: 19-31 years) and twenty-five elderly (15 females and 10 males; 68.8$\pm$2.4 years; age range: 65-74 years) healthy adult subjects were included in this study. Importantly, the elders were highly selected so as to present no cognitive decline compare to young adults [4]. The MEG recordings were performed in the Université Libre de Bruxelles, Hôpital Erasme. The CUB-Hôpital Erasme Ethics Committee approved the study prior to participants' inclusion (references P2011/054 and P2011/151).

The neuromagnetic brain activity was recorded at rest during 5 minutes, with eyes open and gaze fixed on a cross, with a 306-channel whole-scalp MEG system installed in a magnetically shielded room (Neuromag Vectorview & Maxshield™, Elekta Oy, Helsinki, Finland). There are both theoretical and practical reasons to work with eyes open. Since we want to estimate the complexity of the data, we choose the highest complexity possible state, which is eyes open because during eyes closed the strong presence of the alpha rhythm decreases the complexity [31]. From the practical reasons, it is easier to monitor that the subject does not fall asleep, and the ocular artefacts are less complicated and easier to observe with eyes open. The sampling frequency was 1000 Hz, and an online band-pass filtering between 0.1 and 330 Hz was performed.

B. Preprocessing, data-length and parameters, and sensor data reduction

The preprocessing stage consisted of three steps: signal space separation method [32] to reduce external magnetic interferences and correct for head movements, an off-line band-pass filtering (0.1-45 Hz), and removal of physiological artifacts using independent component analysis [33] (FastICA; hyperbolic tangent nonlinearity function; dimension reduction to 30). The band-passing responds to a common practice on MEG data processing. We worked with 50-second segments of continuous data, which represents a compromise between data-length and computational time. For all our experiments on human data, we used a Hann window of 4 seconds for the spectrograms and $\alpha = 2$ for the Rényi entropy.

The 306 sensors of the Neuromag system are arranged into 102 triplets:

$$\{y_{1,m}[n], y_{2,m}[n], y_{3,m}[n]\},\ m = 1, \ldots, 102, \qquad (13)$$

where $y_{1,m}[n]$ and $y_{2,m}[n]$ stands for a pair of orthogonal planar gradiometers, and $y_{3,m}[n]$ stands for a magnetometer. Both kinds of sensors measure different aspects of the magnetic field: magnetometers sample the component normal to the MEG helmet, while gradiometers estimate the tangential gradients of this component. In this work we will only use the planar gradiometers, combining them such that

$$x_m[n] = \sqrt{y_{1,m}^2[n] + y_{2,m}^2[n]},\ m = 1, \ldots, 102. \qquad (14)$$

Effectively, this defines virtual sensors x_m measuring gradiometers amplitude (i.e., the norm of tangential gradients). This affords better interpretability for localization than magnetometers and avoids complications related to gradient orientation.

C. Spatial aggregation approach

In a "multiscale" spirit, we will aggregate sensors at different scales [19]. In that way, we can inquire into real-world phenomena that may only exist as meaningful entities over certain ranges of scale [34]. We will explore different "spatial scales" within the data, for different sizes of neighborhood, gathering amplitude gradiometer sensors around a central sensor location:

$$\mathbf{x}_{\hat{m}}^s[n] = \{x_m[n] \,|\, m \in \mathcal{A}_{\hat{m}}^s\}, \qquad (15)$$

where $\mathcal{A}_{\hat{m}}^s$ is the set composed of the $\hat{m}$-th sensor and the $s-1$ closest to it. Then we proceed treating $\mathbf{x}_{\hat{m}}^s[n]$ as in Eq. (8). In what follows, **scale 1** will refer to the computation of entropies sensor by sensor, using for this the single-channel entropies. **Scale 5** will refer to a neighborhood of $s = 5$ sensors: the central one and the four closest surrounding it. The value is assigned to the central position. This means, treat the five channels as in Eq. (8), with $M = 5$. For **scale 9**: the central sensor and the eight closest to it, assigning the value to the central position (Eq. (8), with $M = 9$).

D. Statistical analysis

We performed two different analyses on our entropy values. First, an analysis *between* groups (i.e. old group vs. young group) on each sensor in order to quantify if there are significant differences. Friedman test were performed on each sensor (25 entropy values per group) with $p < 0.05$, and a Bonferroni correction was applied ($n = 102$).

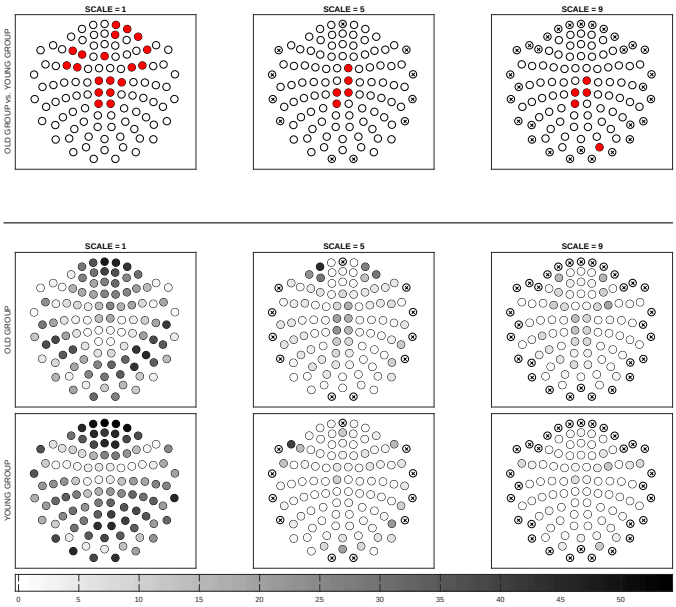

Fig. 2. Multichannel MLSVD entropy for the two groups analyzed at three spatial scales. 50 seconds of continuous data. Spectrograms were performed with Hann window of 4 seconds. Top: Old group vs. Young group. Every red dot represents a significant increase on the entropy of the old group for that sensor. Friedman test, $p < 0.05$, Bonferroni correction. Bottom: Multiple comparison *within* each group and scale for the multichannel MLSVD entropy at three scales. In order to quantify sensor clustering, for every sensor we counted the number of sensors significantly lower from it (Friedman test, $p < 0.05$). The gray level represents this number. Black crosses indicate the sensors that were not center of groups due to peripherality.

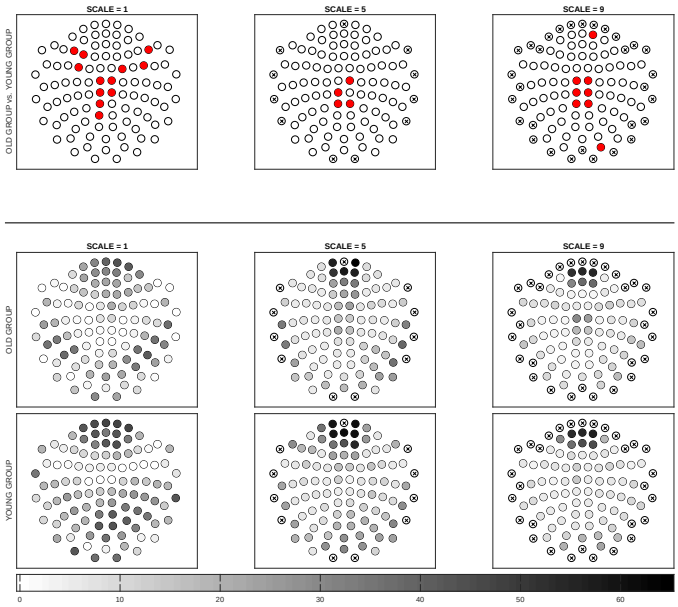

Fig. 3. Multichannel Rényi entropy for the two groups analyzed at three spatial scales. 50 seconds of continuous data. Spectrograms were performed with Hann window of 4 seconds. $\alpha = 2$ for Rényi entropy. Top: Old group vs. Young group. Every red dot represents a significant increase on the entropy of the old group for that sensor. Friedman test, $p < 0.05$, Bonferroni correction. Bottom: Multiple comparison *within* each group and scale for the multichannel Rényi entropy at three scales. In order to quantify sensor clustering, for every sensor we counted the number of sensors significantly lower from it (Friedman test, $p < 0.05$). The gray level represents this number. Black crosses indicate the sensors that were not center of groups due to peripherality.

In a complementary fashion, we also performed an analysis *within* groups. With the goal to see if there is some form of *sensor clustering*, we performed a multiple comparison within each group and spatial scale. Using the `multcompare` tool from MATLAB™, we performed a Friedman test (level of significance of 0.05, corrected for multiple comparisons), and counted for every sensor how many other sensors showed significantly lower entropy values from it. Here, the multiple comparison is made for a given group and a given scale, with 1 value per subject per sensor. In that way, we are looking for sensors with *outstanding* entropy values, i.e. sensors significantly higher from many of the rest of the sensors. If those outstanding sensors happen to be close to each other, then they would constitute a form of cluster.

E. Results

As a first result, we present the application of the MLSVD entropy (which is focused on temporal nonstationarity and similarity across channels) to both the old and young groups (Fig. 2, top panel) at three spatial scales. The red dots indicate significant increases on the entropy for the old group. Significant differences between groups at **scale 1** were located on the midline (frontal and parietal) sensors, and in the more lateral frontal sensors, with a lateralization on the right side, always with higher values for the old group. For **scale 5**, the significant differences were concentrated around the vertex sensor. A similar behavior is observed for **scale 9**, although an occipital sensor also presented a significant difference. Not a single sensor of the old group presented a decrease in entropy.

The bottom panel of Fig. 2 presents the results for the *within* analysis. For **scale 1**, both the old and young groups disclosed important variations across sensors, with the young group exhibiting clusters in the frontal sensors and in the right posterior sensors (both of them also present in the old group, although in a weaker manner). While the old group presented a higher value of entropy in the frontal sensors (Fig. 2, top panel), the young group exhibited a stronger clustering on these sensors, i.e. there is a higher number of outstanding sensors, and these are even more different from the rest of sensors. **Scale 5** disclosed a mild cluster around the vertex sensor and prefrontal sensors in the old group, while no cluster structure was identified on the young group. For **scale 9**, the vertex cluster in the old group is even weaker, and no structure emerged for the young group.

Both *between* and *within* analysis were also performed for the multichannel Rényi entropy (which is focused on the number of components). These results can be appreciated on Fig. 3. The results for the comparison *between* groups were quite similar to those of MLSVD entropy, although at **scale 1** no lateralization effect was observed.

The *within* analysis for the multichannel Rényi entropy (Fig. 3, bottom panel) disclosed a cluster over frontal sensors for the young group at **scale 1**, while this structure was not very clear for the old group. **Scale 5** presented much more defined clusters on the frontal sensors in both groups, with the young

cluster composed of more sensors. The same features were observed for **scale 9**.

IV. Discussion

Our results first show that healthy aging increases TFR entropy values over multiple spatial scales (top panels of Figs. 2 and 3). This is in accordance with the findings reported in [35], where differences in multiscale sample entropy (see [36], [37]) between young and old subjects were found, with the old group presenting larger entropy values, although only for fine temporal scales. However, our results do not depend on the temporal scales, but they reflect the changes in all the frequency bandwidth and are consistent across spatial scales. Increased complexity of MEG signals with age were also reported in [8] and [9]. Evidences of aging-related changes in the Fourier spectrum of EEG with a decrease in power for low frequencies and an increase for high frequencies were also reported in [38], [39], [40]. This "flattening" of the spectrum leads to an increase in the spectral (or Wiener) entropy [41]. The fact that the differences between groups are not confined to a particular region but can be found on central, frontal and occipital (scale 9, Figs. 2 and 3) regions might be due to the flattening of the spectrum being usually evidenced in the majority of the sensors, and not in a specific region. However, the significant differences (marked with red dots) tend to be more centrally located for scales 5 and 9, for which a frontal significant sensor appears only for Rényi entropy. The aggregation of sensors "faded" some differences between groups and also reduced the lateralization effects. This suggests that the major differences between groups are expected to be observed at the finest spatial scales.

As in [4], we also performed here a power spectral analysis, although at sensor level. From the virtual sensors $x[n]$ from Eq. (14), we computed the discrete Fourier transform $X[k] = \sum_n x[n]\exp(-i2\pi k\Delta f n)$, and the spectral power in three specific bands: $P_{band} = \sum_{k\in band} |X[k]|^2$; for theta (4-8 Hz), alpha (8-13 Hz) and beta (13-25 Hz) bands. The results can be appreciated in Fig. 4. While the theta band presents only two significant sensors, the alpha band does not show significant differences at all. The beta band presents three significant sensors. This result evidences the limitations of classical power spectral analysis, while possing interpretations issues: three different results related to three different frequency bands that must be discussed. The interpretation of different band-specific results emerging from a single structural network is still an ongoing debate [42]. On the contrary, the analysis proposed in this work does not rely on classical frequency bands, offering a single result. It is also more sensitive for the task of identifying significant age-related changes on neuromagnetic activity.

The analysis *within* groups offers a possibility to look for some forms of *sensor clustering*. The aggregation of sensors at larger scales (5 and 9) for Rényi entropy allows us to see this phenomenon in the frontal sensors of both groups, which was not that clearly defined for scale 1, as the darker colors for scales 5 and 9 indicate (Fig. 3, bottom panel). At larger scales, the distribution of the number of components of the magnetic activity (as measured by the multichannel Rényi entropy, Fig. 3) forms less defined clusters in the frontal sensors of the old group. At the same time, the nonstationarity of the magnetic activity (as measured by the MLSVD entropy, Fig. 2, bottom panel, scale 1) presents a more defined cluster in the frontal sensors of the young group. The *within* analysis reveals that, while the old group has more complex TFRs in most of the sensors (as disclosed by the *between* analysis), the distribution of the values *across* sensors is more complex (with greater variation) for the young group.

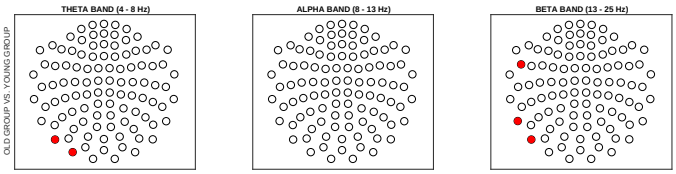

Fig. 4. Power spectral analysis for the two groups at three frequency bands. Every red dot represents a significant difference for that sensor. Friedman test, $p < 0.05$, Bonferroni correction.

The differences between groups that we found here, which do not reflect changes in electrophysiological resting-state networks, in contrast to the power envelope correlation results reported in [4], suggests that complexity studies another aspect than power envelope-based connectivity, that is more sensitive to age-related changes and possibly to brain disorders. However, while the envelope connectivity analysis reported in [4] was performed at the level of brain sources, the results presented here were obtained at the sensor level. Being the former analysis more "local" than the latter one, it might be that some scale effect makes age-related differences to express better at sensor scale 1.

The *within* groups analysis of entropy measures intends to quantify clustering: groups of adjacent sensor significantly higher from the rest. Whether a cluster of sensors is related to a local network should be further investigated since we are discarding here the field spread effect [43]. This question could be addressed in computing a mutual information based on the complexity measures presented here. We would be moving towards a time-frequency complexity-based connectivity approach that, when compared with the approaches based on phase or power-envelope, might bring novel aspects to brain connectivity. We would have to make use of the new multichannel entropies here introduced, along with their single-channel counterparts [15].

Technical Limitations. Our study presents limitations since it is limited to the sensor level. The analysis at the source level will be addressed in future works.

V. Conclusions

We introduced new multichannel time-frequency complexity measures. We illustrated their properties on artificial signals, and applied them to a particular real-world problem: the study of healthy aging *via* MEG recordings.

Differences between the two groups emerged. Healthy aging is characterized by higher complexity, which confirms previous results. The complexity measures here introduced seem to be a better indicator of the neurophysiologic changes of aging

than power-envelope connectivity, and classical band-specific power spectral analysis. Moreover, since they do not make use of the classical band-pass filtering, they retrieve a single results reflecting all the richness of the frequency content.

The aggregation of sensors at larger scales evidenced some form of clustering in the frontal part. This phenomenon deserves attention for future studies, especially in relation to functional connectivity, to which we will apply our methods in the near future, with a mutual information approach based on our time-frequency complexity measures.

ACKNOWLEDGMENTS

This work was supported by the European Commission, Project FP7 DESIRE (Health-F2-602531-2013). M. A. Colominas and M. El Sayed Hussein Jomaa are both full-time granted by the DESIRE project.

N. Coquelet is supported by a research grant from the ULB ARC Consolidation 2014-2017 "Characterization of the electrophysiological bases, the temporal dynamics and the functional relevance of resting state network", and by the research convention "Les Voies du Savoir" (Fonds Erasme, Brussels, Belgium). The MEG project at the CUB-Hôpital Erasme is financially supported by the Fonds Erasme (Brussels, Belgium) via the research convention "Les Voies du Savoir".

REFERENCES

[1] M. D. Greicius *et al.*, "Functional connectivity in the resting brain: a network analysis of the default mode hypothesis," *Proc. National Academy of Sciences*, vol. 100, no. 1, pp. 253–258, 2003.

[2] E. Pekkonen, "Mismatch negativity in aging and in Alzheimer's and Parkinson's diseases," *Audiology and Neurotology*, vol. 5, no. 3-4, pp. 216–224, 2000.

[3] P. M. Rossini *et al.*, "Clinical neurophysiology of aging brain: from normal aging to neurodegeneration," *Progress in Neurobiology*, vol. 83, no. 6, pp. 375–400, 2007.

[4] N. Coquelet *et al.*, "The electrophysiological connectome is maintained in healthy elders: a power envelope correlation MEG study," *Scientific Reports*, vol. 7, 2017.

[5] M. Hämäläinen *et al.*, "Magnetoencephalography - theory, instrumentation, and applications to noninvasive studies of the working human brain," *Reviews of Modern Physics*, vol. 65, no. 2, p. 413, 1993.

[6] F. De Pasquale *et al.*, "Temporal dynamics of spontaneous MEG activity in brain networks," *Proc. National Academy of Sciences*, vol. 107, no. 13, pp. 6040–6045, 2010.

[7] R. Sala-Llonch *et al.*, "Reorganization of brain networks in aging: a review of functional connectivity studies," *Frontiers in Psychology*, vol. 6, 2015.

[8] A. Fernández *et al.*, "Brain oscillatory complexity across the life span," *Clinical neurophysiology*, vol. 123, no. 11, pp. 2154–2162, 2012.

[9] E. Shumbayawonda *et al.*, "Permutation entropy for the characterisation of brain activity recorded with magnetoencephalograms in healthy ageing," *Entropy*, vol. 19, no. 4, p. 141, 2017.

[10] E. Shumbayawonda *et al.*, "Complexity Changes in Brain Activity in Healthy Ageing: A Permutation Lempel-Ziv Complexity Study of Magnetoencephalograms," *Entropy*, vol. 20, no. 7, p. 506, 2018.

[11] M. J. Brookes *et al.*, "Investigating the electrophysiological basis of resting state networks using magnetoencephalography," *Proc. National Academy of Sciences*, vol. 108, no. 40, pp. 16 783–16 788, 2011.

[12] J. F. Hipp *et al.*, "Large-scale cortical correlation structure of spontaneous oscillatory activity," *Nature neurosci.*, vol. 15, no. 6, p. 884, 2012.

[13] V. Wens *et al.*, "About the electrophysiological basis of resting state networks," *Clin. Neurophysiol.*, vol. 125, no. 8, pp. 1711–1713, 2014.

[14] R. G. Baraniuk *et al.*, "Measuring time-frequency information content using the Rényi entropies," *IEEE Trans. Information Theory*, vol. 47, no. 4, pp. 1391–1409, 2001.

[15] M. A. Colominas *et al.*, "Time-varying time-frequency complexity measures for epileptic EEG data analysis," *IEEE Trans. Biomedical Engineering*, vol. 65, no. 8, pp. 1681–1688, 2018.

[16] P. L. Nunez, "Toward a quantitative description of large-scale neocortical dynamic function and EEG," *Behavioral and Brain Sciences*, vol. 23, no. 3, pp. 371–398, 2000.

[17] F. Varela *et al.*, "The brainweb: phase synchronization and large-scale integration," *Nature reviews neuroscience*, vol. 2, no. 4, p. 229, 2001.

[18] M. Siegel *et al.*, "Spectral fingerprints of large-scale neuronal interactions," *Nature Reviews Neuroscience*, vol. 13, no. 2, p. 121, 2012.

[19] S. Mallat, *A wavelet tour of signal processing: the sparse way*. Academic press, 2009.

[20] H.-T. Wu *et al.*, "Using synchrosqueezing transform to discover breathing dynamics from ECG signals," *Applied and Computational Harmonic Analysis*, vol. 36, no. 2, pp. 354–359, 2014.

[21] X. Zhang *et al.*, "A new approach for crude oil price analysis based on empirical mode decomposition," *Energy Economics*, vol. 30, no. 3, pp. 905–918, 2008.

[22] R. Carmona *et al.*, "Multiridge detection and time-frequency reconstruction," *IEEE Trans. Signal Processing*, vol. 47, no. 2, pp. 480–492, 1999.

[23] ——, "Characterization of signals by the ridges of their wavelet transforms," *IEEE Trans. Signal Processing*, vol. 45, no. 10, pp. 2586–2590, 1997.

[24] T. Oberlin *et al.*, "Second-order synchrosqueezing transform or invertible reassignment? Towards ideal time-frequency representations," *IEEE Trans. Signal Processing*, vol. 63, no. 5, pp. 1335–1344, 2015.

[25] W. J. Williams *et al.*, "Uncertainty, information, and time-frequency distributions," in *San Diego,'91, San Diego, CA*. International Society for Optics and Photonics, 1991, pp. 144–156.

[26] N. Saulig *et al.*, "Instantaneous counting of components in nonstationary signals," in *2013 Proc. 21st Eur. Signal Proc. Conf. (EUSIPCO)*. IEEE, 2013, pp. 1–5.

[27] O. Alter *et al.*, "Singular value decomposition for genome-wide expression data processing and modeling," *Proc. National Academy of Sciences*, vol. 97, no. 18, pp. 10 101–10 106, 2000.

[28] B. Boashash *et al.*, "Time-frequency processing of nonstationary signals: advanced TFD design to aid diagnosis with highlights from medical applications," *IEEE Signal Processing Magazine*, vol. 30, no. 6, pp. 108–119, 2013.

[29] L. De Lathauwer *et al.*, "A multilinear singular value decomposition," *SIAM journal on Matrix Analysis and Applications*, vol. 21, no. 4, pp. 1253–1278, 2000.

[30] N. Vervliet *et al.*, "Tensorlab 3.0," *available online, URL: www.tensorlab.net*, 2016.

[31] C. J. Stam *et al.*, "Dynamics of the human alpha rhythm: evidence for non-linearity?," *Clinical Neurophysiology*, vol. 110, no. 10, pp. 1801–1813, 1999.

[32] S. Taulu *et al.*, "Applications of the signal space separation method," *IEEE Trans. on Signal Processing*, vol. 53, no. 9, pp. 3359–3372, 2005.

[33] A. Hyvärinen *et al.*, *Independent component analysis*. John Wiley & Sons, 2004, vol. 46.

[34] T. Lindeberg, "Scale-space: a framework for handling image structures at multiple scales," 1996.

[35] A. McIntosh *et al.*, "Spatiotemporal dependency of age-related changes in brain signal variability," *Cerebral Cortex*, vol. 24, no. 7, pp. 1806–1817, 2014.

[36] M. Costa *et al.*, "Multiscale entropy analysis of complex physiologic time series," *Physical review letters*, vol. 89, no. 6, p. 068102, 2002.

[37] M. Costa *et al.*, "Multiscale entropy analysis of biological signals," *Physical review E*, vol. 71, no. 2, p. 021906, 2005.

[38] C. Babiloni *et al.*, "Sources of cortical rhythms in adults during physiological aging: a multicentric EEG study," *Human Brain Mapping*, vol. 27, no. 2, pp. 162–172, 2006.

[39] E. L. Vlahou *et al.*, "Resting-state slow wave power, healthy aging and cognitive performance," *Scientific Reports*, vol. 4, 2014.

[40] L. Waschke *et al.*, "States and traits of neural irregularity in the age-varying human brain," *Scientific Reports*, vol. 7, no. 1, p. 17381, 2017.

[41] G. Powell and I. Percival, "A spectral entropy method for distinguishing regular and irregular motion of Hamiltonian systems," *Journal of Physics A: Mathematical and General*, vol. 12, no. 11, p. 2053, 1979.

[42] P. Tewarie *et al.*, "How do spatially distinct frequency specific MEG networks emerge from one underlying structural connectome? The role of the structural eigenmodes," *NeuroImage*, vol. 186, pp. 211–220, 2019.

[43] J.-M. Schoffelen and J. Gross, "Source connectivity analysis with MEG and EEG," *Human brain mapping*, vol. 30, no. 6, pp. 1857–1865, 2009.